ELSEVIER

Contents lists available at ScienceDirect

Acta Biomaterialia

journal homepage: www.elsevier.com/locate/actbio



Full length article

Feasibility evaluation of a Cu-38 Zn alloy for intrauterine devices: In vitro and in vivo studies



Kun Wang^{a,b,1}, Guo Bao^{a,1}, Qianqian Fan^{a,b}, Liquan Zhu^{a,b}, Lijun Yang^{a,b}, Tingting Liu^{a,b}, Zechuan Zhang^c, Guannan Li^c, Xihua Chen^a, Xiangbo Xu^{a,*}, Xiaoxue Xu^{d,*}, Bin He^{a,*}, Yufeng Zheng^{c,e,*}

- ^a Department of Reproduction and Physiology, National Research Institute for Family Planning, Beijing 100081, China
- ^b Graduate School of Peking Union Medical College, Beijing 100730, China
- ^c School of Materials Science and Engineering, Peking University, Beijing 100871, China
- d Institute for Biomedical Materials and Devices, Faculty of Science, University of Technology Sydney, NSW 2007, Australia
- e International Research Organization for Advanced Science and Technology, Kumamoto University, 2-39-1 Kurokami, Chuo-Ku, Kumamoto 860-8555, Japan

ARTICLE INFO

Article history: Received 16 June 2021 Revised 29 October 2021 Accepted 4 November 2021 Available online 11 November 2021

Keywords:
Cu-Zn alloy
Simulated uterine fluid
Burst release
Biocompatibility
Corrosion behavior
Copper-containing intrauterine devices

ABSTRACT

The existing adverse effects of copper in copper-containing intrauterine devices (Cu-IUDs) have raised concerns regarding their use. These adverse effects include burst release of cupric ions (Cu²⁺) at the initial stage and an increasingly rough surface of the Cu-IUDs. In this study, we investigated the use of two copper alloys, Cu-38 Zn and H62 as the new upgrading or alternative material for IUDs. Their corrosive properties were studied in simulated uterine fluid (SUF) by using electrochemical methods, with pure Cu as a control. We studied the in vitro long-term corrosion behaviors in SUF, cytotoxicity to uterine cells (human endometrial epithelial cells and human endometrial stromal cells), in vivo biocompatibility and contraceptive efficacy of pure Cu, H62, and Cu-38 Zn. In the first month, the burst release rate of Cu²⁺ in the Cu-38 Zn group was significantly lower than those in the pure Cu and H62 groups. The in vitro cytocompatibility Cu-38 Zn was better than that of pure Cu and H62. Moreover, Cu-38 Zn showed improved tissue biocompatibility in vivo experiments. Therefore, the contraceptive efficacy of the Cu-38 Zn is still maintained as high as the pure Cu while the adverse effects are significantly eased, suggesting that Cu-38 Zn can be a suitable potential candidate material for IUDs.

Statement of significance

The existing adverse effects associated with the intrinsic properties of copper materials for coppercontaining intrauterine devices (Cu-IUD) are of concern in their employment. Such as, burst release of cupric ions (Cu²⁺) at the initial stage and an increasingly rough surface of the Cu-IUD. In this work, Cu alloyed with a high amount of bioactive Zn was used for a Cu-IUD. The Cu-38 Zn alloy exhibited reduced burst release of Cu²⁺ within the first month compared with the pure Cu and H62. Furthermore, the Cu-38 Zn alloy displayed significantly improved biocompatibility and a much smoother surface. Therefore, high antifertility efficacy of the Cu-38 Zn alloy was well maintained, while the adverse effects are significantly eased, suggesting that the Cu-38 Zn alloy is promising for a Cu-IUD.

© 2021 Acta Materialia Inc. Published by Elsevier Ltd. All rights reserved.

E-mail addresses: Xiangboxuhappy@126.com (X. Xu), Xiaoxuehelen.xu@uts.edu.au (X. Xu), hebin@nrifp.org.cn (B. He), yfzheng@pku.edu.cn (Y. Zheng).

¹ Kun Wang and Guo Bao contributed equally to this study.

1. Introduction

Copper-containing intrauterine devices (Cu-IUDs) are the safe, long-term effective, and reversible contraception tools that have been used extensively worldwide for population control [1,2]. Cu-IUDs have a satisfactory contraception efficacy and a high usage rate. However, the undesirable adverse effects of the existing Cu-IUDs such as irregular bleeding, spotting, pelvic pain and infection

^{*} Corresponding authors: School of Materials Science and Engineering, Peking University, No.5 Yi-He-Yuan Road, Hai-Dian District, Beijing 100871, China.

limit their usage [3–6]. These adverse effects are associated with the inherent corrosive behavior of Cu, such as including the burst release of cupric ions (Cu²⁺) in the first few months [7–9] and increased roughness of the material surface due to long-term corrosion in the uterine cavity [10].

Various attempts have been made to solve the existing problems associated with Cu-IUDs, such as by changing the shape and size of copper components [11,12] or by adding non-steroidal anti-inflammatory drugs in the device [13,14]. However, the results have been unsatisfactory. Other than the structural modifications of Cu-IUDs, new types of Cu-IUDs have been developed using polymers of Cu or nano/microparticles composites of Cu with controlled release of Cu2+ rather than Cu bulk metal as the active material. Xie et al. [15-17] designed Cu/low-density polyethlene nanocomposites. Li et al. [18-20] developed a new type of crosslinked composite cupric chloride/ silicon dioxide/poly (vinyl alcohol) (CuCl₂/SiO₂/PVA). Although the polymer composite-based IUDs have enabled the controlled release of Cu²⁺, other concerns such as poor mechanical properties, complex fabrication process, sensitive surface functional groups and unstable internal structure of the polymer were raised [17,21,22], Furthermore, Xu et al. created fabricated ultrafine- grained copper (UFG Cu) by using the equal-channel angular extrusion (ECAP) technique and used it as the active material for the Cu-IUD. A lower Cu²⁺ burst release was observed in UFG Cu than that in coarse-grained copper; however, UFG Cu was highly cytotoxic. Hence, the clinical application of UFG Cu in Cu-IUDs presents challenges, and more studies are warranted to identify suitable potential candidate Cu materials for Cu-IUD.

In the present study, we propose the use of alloys of Cu and other metal to reduce the bio-corrosion and increase the biocompatibility of Cu-IUDs. Zinc (Zn) is the second most abundant trace element in the human body that participates in various enzymatic and metabolic processes [23]. Meanwhile, it possesses contraceptive [24], wound healing [25], and antibacterial properties [26]. A combination of Cu^{2+} and zinc ions (Zn^{2+}) was found to have an antagonistic effect on the cytotoxicity and a synergistic effect on the antibiotic activity [27]. Therefore, the use of Zn in copper alloys to design IUDs can improve the efficacy, adaptability and antibacterial activity of these devices, promote endometrial repair, and prevent abnormal uterine bleeding.

The present study attempted to reduce the initial burst release of Cu^{2+} and minimize the adverse effects of the existing Cu-IUDs. Our study proposes a novel Cu-38 Zn alloy as a potential candidate for the IUDs. We used industrial H62 alloy as a control. We studied the bio-corrosion properties, in vitro cytocompatibility, and in vivo histocompatibility of the Cu-38 Zn alloy, H62 alloy, and pure Cu. We also performed antifertility experiments to evaluate the contraceptive efficacy of Cu-38 Zn alloy.

2. Materials and methods

2.1. Material preparation

Pure copper (99.99%) and commercial H62 (62.5 wt.% Cu, 0.12 wt.% Fe, 0.07 wt.% Pb, remainder Zn) rods of 10 mm diameter and 1 m length were purchased from Yuandelai Industrial Materials Co. (Shenzhen, China) and Meihang Copper & Aluminum Co. (Shenzhen, China), respectively. The as-cast Cu-38 Zn alloys (38.5 wt.% Zn, remainder Cu) was prepared in the Hunan Rare-Earth Material Research Institute. All the experimental samples were sliced in discs 10 mm in diameter and 2 mm thickness.

2.2. Microstructure characterization

For the microstructure observation, the Cu samples were ground to 2000 grits by using silicon carbide (SiC) paper, fol-

lowed by polishing it with 3 μ m and 50 nm colloidal silicon dioxide (SiO₂) suspensions. Electron backscatter diffraction (EBSD) analysis was performed using an FEI Helios G4 PFIB UXe DualBeam scanning electron microscope and interpreted using 'CHANNEL 5' EBSD software. The data were analysed using Aztec analysis software. Field-Emission scanning electron microscope (Zeiss, Supra 55VP) equipped with an energy dispersive X-ray spectrometer was used to observe the surface of the materials and analysis the elemental composition.

2.3. Electrochemical measurement

The electrochemical tests were performed using a typical threeelectrode cell with a platinum plate as the counter-electrode, a saturated calomel electrode as the reference electrode, and a Cu specimen as the working electrode. The tests were performed in a simulated uterine fluid (SUF) solution at 37 ± 0.5 °C by using an electrochemical workstation ((Autolab, Metrohm, Switzerland). Each sample was mechanically polished with SiC paper to obtain 2000 grits. It was then ultrasonically cleaned for 15 min in acetone and ethanol. The exposure area of the specimen was 0.242 cm². Each specimen was monitored under an open circuit potential (OCP) for approximately 0.5 h. The potentiodynamic polarization measurements were evaluated at a scan rate of 1 mV/s. Similarly, we measured five different samples. Electrochemical parameters including OCP, corrosion potential (E_{corr}), and corrosion current density (i_{corr}) were calculated from the polarization curves through the Tafel analysis.

2.4. Long-term immersion test

The long-term corrosion behaviors of Cu, Cu-38 Zn, and H62 samples were identified in the SUF solution (comprising NaCl 4.97 g/L; KCl 0.224 g/L; CaCl₂ 0.167 g/L; NaHCO₃ 0.25 g/L; Glucose 0.5 g/L and NaH₂PO₄•2H₂O 0.072 g/L), according to the method described by ASTM-G31-72 at 37 °C for 300 days, with a SUF volume to specimen exposure surface area ratio of 20 mL/cm². Before the experiment, all the samples were mechanically polished with SiC paper to 2000 grits and then ultrasonically cleaned for 15 min in acetone and ethanol. The initial pH of the SUF solution was adjusted to 7.0 (PB-10, Sartorius). The pH of the SUF solution and the released Cu²⁺ and Zn²⁺ during the immersion tests were detected on the 1st, 10th, 20th, 30th, 45th, 60th, 90th, 120th, 150th, 180th, 210th, 240th, 270th and 300th day. The ion concentrations in the SUF solutions were measured using inductively coupled plasma atomic emission spectrometry (ICP-OES, iCAP6300, Thermo Scientific). The metallic ion release rates are expressed as microgram per day (µg/day).

After being immersed for 1, 10, 30, 60, 150, and 300 days, the Cu and Cu alloy samples were taken out from the SUF solution, and these samples were fully rinsed and air-dried. The corrosion rate was calculated by measuring the sample weight before and after immersion in the SUF solution. The corroded layer was removed by immersing the samples in the concentrated hydrochloric acid for 3 min, according to the method described by ASTM G1–03 [28]. The corrosion rate was calculated using the following equation:

$$C = \frac{\Delta m}{\rho \times A \times t}$$

where C is the corrosion rate in mm/year, Δm is the weight loss in grams, ρ is the material density in g/cm^3 , A is the initial exposed surface area in cm^2 , and t is the time of immersion in days (d). At least four measurements were taken for each group.

2.5. Corrosion morphology and composition characterization

The surface morphologies and composition of the long-term immersed Cu and Cu alloy samples were characterized through scanning electron microscopy (SEM, S-4800 Emission Scanning electron microscopy, Hitachi, Japan) equipped with an energy dispersive X-ray spectrometer (EDS, Bruker Quantax, Germany). The surface phase analysis was performed using the X-ray diffraction technique (XRD, Rigaku DMAX 2400, Japan), with Cu-K α radiation at a scan rate of 4 °C/min operated at 40 kV and 100 mA. The chemical composition of the corroded products was identified using an X-ray photoelectron spectroscope (XPS, Axis Ultra Analytical, Britain) with AlK α radiation.

2.6. In vitro studies

2.6.1. Cell culture and immunofluorescence assay

Human endometrial epithelial cells (HEECs) and human endometrial stromal cells (HESCs) were used to detect the cytocompatibility of Cu and Cu alloys. All cell lines were purchased from Bnbio Company (Beijing, China). HEECs and HESCs were cultured in Dulbecco's Modified Eagle medium containing Nutrient Mixture F-12 (DMEM/F12, Gibco, USA), 10% foetal bovine serum (FBS, Gibco, Australia), $100\,\text{U/mL}$ penicillin, and $100\,\text{µg/mL}$ streptomycin (Gibco, USA). The cells were incubated in a humidified atmosphere with 5% CO₂ at $37\,^{\circ}\text{C}$.

For the immunofluorescent assay, both types of cells were cultured on coverslips and fixed with methanol/acetone (1:1, v/v) for 15 min at $-20~^{\circ}$ C, washed three times (5 min for each time) with phosphate-buffered saline (PBS), and then permeabilised with 0.2% Triton-X-100 in PBS for 5 min at room temperature. Nonspecific protein binding was blocked by adding 3% bovine serum albumin at room temperature for 1 h. Monoclonal anti-cytokeratin, or anti-vimentin actin antibody was added to the cells, and the coverslips were kept at 4 $^{\circ}$ C overnight. The next day, the cells were washed with PBS and incubated with the corresponding secondary anti-bodies for 2 h at room temperature in dark. The cell structures were visualized using a fluorescence microscope, as shown in Fig. S1

2.6.2. Cytotoxicity test

The in vitro cytotoxicity of Cu and Cu alloys was determined using an indirect cell assay. The polished Cu samples were first rinsed and air dried. Each side of the samples was placed under ultraviolet radiation (UV) for at least 2 h. The sample extracts were prepared according to the method described by ISO 10,993–12: 2012 [29]. The samples were incubated in the cell culture medium at a volume to area ratio of 1.25 cm²/mL. The extracts were incubated at 37 °C, under 5% CO₂ for 24 h and were then centrifuged and stored at 4 °C. The positive control cell culture was added with 10% dimethylsulfoxide (DMSO, Sigma-Aldrich, USA), and negative control cell culture was added with the conventional medium. The pH and ion concentrations of the extracts were measured using a pH meter and an inductively coupled plasma optical emission spectrometer (ICP-OES), respectively.

The cells were seeded in 96-well cell culture plates at a density of 1×10^4 cells per 100 μL medium. The plates were then incubated for 24h to allow the attachment of cells. The next day, the extracts were added to each well, and plates were incubated for 1, 2, and 3 days. Then, the extracts were replaced with a cell culture medium containing 10% Cell Counting Kit-8 (CCK8, Dojindo Molecular Technologies, Japan) solution and subsequently incubated at 37 °C for 1 h. A microplate reader (Bio-Rad 680) was used to measure the absorbance of the solution in each well at a wavelength of 450 nm.

2.7. In vivo studies

2.7.1. Animal care

Sexually mature female Sprague-Dawley (SD) rats (8–10 weeks old, weight 200–240 g) were obtained from the Beijing Vital River Laboratory Animal Technology Co. Ltd (Beijing, China). The Animals were acclimatized to the laboratory conditions for one week prior to the experiments. They were bred under standard conditions and provided access to conventional food and drinking water ad libitum. All the protocols were approved by the Ethical Committee of the National Research Institute for Family Planning.

2.7.2. Animal treatment

We adopted rats to analyze the contraceptive efficacy of the Cu and Cu alloy materials following a large volume of previous reports [30–32]. In total, 48 sexually mature female SD rats were randomly assigned to the following four groups (n=12 for each group): sham-operated group (SO group), pure Cu group (Cu group), H62 group, and Cu-38 Zn group. The SD rats in the Cu, H62, and Cu-38 Zn groups were anesthetized. Each corresponding material of 1 mm diameter and 10 mm length was implanted in the uterine cavity and fixed on the uterine wall of the SD rats. In the SO group, SD rats underwent similar surgical procedures but without their insertion of Cu materials in the uterine cavity. The activity, standard diet and health status of all the SD rats were closely monitored during experimentation.

2.7.3. Histological analysis

The uterine tissues of the SD rats were collected for histological analysis after 3, 7, 14, and 28 days of implantation. Uterine tissue samples were fixed in 4% (w/v) paraformaldehyde (Sigma-Aldrich, USA), dehydrated using a series of ethanol (70%, 75%, 80%, 95% I and II, and 100% I and II), placed in xylene, embedded in paraffin blocks, and sliced into 5 µm sections. Paraffin-embedded tissue sections were deparaffinized by immersing them in xylene and rehydrated in a decreasing concentration of ethanol (100% I and II, 95% I and II, 80%, 75%, and 70%). Finally, the sections from each sample were stained with haematoxylin-eosin (H&E). Images of the stained sections were obtained using an optical microscope (XS-23C, PuZhe Thotoelectric, China). Tissues sections were stained with H&E to determine the compatibility of the tissues with the Cu samples and the extent of inflammatory response and tissue damage.

2.7.4. Antifertility experiment

A total of 40 sexually mature female SD rats were randomly divided into the following five groups: normal control group (n=5), SO group (n=5), pure Cu group (n=10), H62 group (n=10), and Cu-38 Zn group (n=10). We are determined the oestrous cycle stage from the histological examination of the vaginal smears. Fifteen days after Cu materials insertion, pro-oestrous female rats were selected to mate with fertile males. The female SD rate were evaluated for the presence of vaginal plugs the following morning. The day on which the vaginal plug was observed and designated as day 0.5 (D 0.5) of pregnancy. The pregnant SD rats were sacrificed, and the pregnancy outcome was observed at D 11.5.

2.7.5. Observation of the Cu and Cu alloys after being implanted

The implanted Cu materials were removed from the SD rats at 3, 7, 14, and 28 days after insertion. The surface morphologies and compositions of the corroded product were examined through SEM coupled with EDS. Three samples were examined at each time point for each type of Cu material in this experiment.

2.8. Statistical analysis

Data are reported as mean $(x)\pm$ standard deviation $(x\pm SD)$. Oneway analysis of variance was used to determine the statistically significant difference, which was followed by the Tukey post hoc tests. P values of <0.05 were considered statistically significant unless noted otherwise.

3. Results

3.1. Microstructural study

Microstructures of pure Cu, Cu-38 Zn, and H62 were characterized using the EBSD, SEM, and EDS techniques, as shown in Fig. 1. We observed an area of pure Cu surface in the EBSD image, as shown in Fig. 1a-(I). we also observed the presence of randomly orientated grains with relatively uniform sizes. The size of the grains ranged from 0.13 to 2.14 µm. As shown in Fig. 1a-(II), the majority of the EDS peaks attributed to Cu, with a trace amount of Si and O from the polishing agent SiO2, and a trace amount of C from the ambient environment. The predominant presence of Cu in the EDS spectrum suggested the purity of the Cu material. Fig. 1a-(III) shows the elemental mapping of the square area in the Cu surface, as shown in Fig. 1a-(I). The intensity of the Cu signal was evenly distributed within the whole area, which indicates that Cu is uniformly present without segregations. As shown in Fig. 1b-(I), the low magnification SEM image reveals an area of Cu-38 Zn alloy with distinctly different phases. The two main phases show a difference in contrast with scattered dark spots. Fig. 1b-(II) shows grain boundaries at high magnification. The grains were in an elongated shape, with approximately 0.1-0.2 µm width and $\geq 1 \, \mu m$ length. Some small grains of \sim approximately 50 nm size were also present. Fig. 1b-(III) corresponds to the square area from Fig. 1b-(I) and shows clear phase boundaries. The EDS spectrum in Fig. 1b-(IV) corresponds to the entire area from Fig. 1b-(III), and it represents the main elements Cu and Zn. The concentrations of Cu and Zn were quantitatively analyzed. We found the two phases contained different Zn concentrations, 39.5 wt.% in the dark area and 45.3 wt.% in the bright area. In the equilibrium phase diagram, the Cu-Zn solid solution covered a wide range, with 38.95 wt.% Zn. Above this Zn content, the intermetallic β -CuZn (CsCl type) would be formed [33,34]. Fig. 1b-(V and VI) are the Cu and Zn elemental mapping of the entire area from Fig. 1b-(III). The two phases can be differentiated from the contrast of the SEM image (1b-(I & III)) that presents Cu-rich phase in the dark area and the Zn rich phase in the bright area. The low-magnification SEM image in Fig. 1c-(I) shows different phases of the H62 sample. Fig. 1c-(II) shows highmagnification distinct phases and grain boundaries with randomly shaped grains of size 0.1 - 1.5 µm. We also observed some small grains of size 50 - 100 nm. Fig. 1c-(III) is the combined elemental mapping image of Cu, Zn, Pb, and Fe, corresponding to the squared area in Fig. 1c-(I). Cu and Zn were found to be distributed uniformly within the whole area, whereas Pb was concentrated in the center spot. This observation confirmed that Pb precipitated as a particle. Fe also existed in the small spots; however, its low intensity suggested a low Fe concentration. The EDS spectrum in Fig. 1c-(IV) corresponds to the whole area of Fig. 1c-(III), which confirmed that the main elements are Cu and Zn, with a trace amount of Pb and Fe. Fig. 1c-(V & VI) depict the individual Cu and Pb elemental mapping.

3.2. Immersion tests

Fig. 2a shows the release rate of Cu^{2+} from Cu, Cu-38 Zn, and H62 materials in the SUF solution for 300 days at 37 °C. As shown in Fig. 2a, within the first 30 days of immersion, the initial burst

Table 1 Electrochemical parameters of pure Cu, H62 and Cu-38Zn in SUF solution.

Materials	$I_{\rm corr}~(\mu A/{\rm cm}^2)$	$E_{\rm corr}$ (V)	Corrosion rate (mm/year)
Cu	3.520±0.226	-0.201 ± 0.008	$0.041\pm0.003 \\ 0.012\pm0.002^* \\ 0.014\pm0.004^*$
H62	1.065±0.201*	-0.197 ± 0.003	
Cu-38Zn	1.198±0.347*	-0.194 ± 0.001	

^{*}P<0.05 when compared with the pure Cu group.

release rate of Cu²⁺ from pure Cu was significantly higher than that from the Cu-38 Zn and H62 alloys. However, the burst release rate of Cu^{2+} from the Cu-38 Zn was lesser than that from the H62. The initial Cu^{2+} release rates were 12.24 µg/day, 21.53 µg/day, and 38.91 µg/day from Cu-38 Zn, H62 and pure Cu, respectively. During the steady release phase between the days 60 - 300, we observed constant slow Cu²⁺ release rates of 0.68 µg/day, 0.60 µg/day, and 0.93 µg/day from Cu-38 Zn, H62 and pure Cu, respectively. The long-term release profiles of Zn²⁺ from Cu-38 Zn and H62 samples are shown in Fig. 2b. The release of Zn²⁺ from Cu-38 Zn and H62 samples showed two phases, similar to the Cu²⁺ release, which included an initial burst release phase and a relatively stable release phase. The high release rate of Zn2+ in the initial day was accompanied by the burst release of Cu^{2+} . The initial Zn^{2+} release rates from Cu-38 Zn and H62 were $6.9\,\mu\text{g}/\text{day}$ and $9.2\,\mu\text{g}/\text{day}$, respectively. The long-term Zn²⁺ release rate from Cu-38 Zn and H62 gradually became steady after 90 days of immersion, which was maintained at approximately 0.56 µg/day and 0.26 µg/day, respectively.

The weight-loss method was used to calculate the corrosion rate of the three Cu materials during immersion, as shown in Fig. 2c. The corrosion rate of the Cu materials was significantly high in the first 30 days of immersion, especially for the pure Cu. The corrosion rates decreased for all Cu materials upon prolonged immersion. Both Cu-38 Zn and H62 corroded much slower than pure Cu at all time points. This result indicated that the corrosion resistance of Cu-38 Zn and H62 is better than that of pure Cu.

3.3. Electrochemical measurements

Each specimen was monitored under an OCP for approximately 0.5 h. The potentiodynamic polarization curves of the samples in the SUF solution were obtained, shown in Fig. 3. To minimize the variations, the Tafel slopes were carefully determined in the potential range of $70-200\,\mathrm{mV}$ away from Ecorr on both the cathodic curve and the anodic curves. The corresponding electrochemical parameters are presented in Table 1. No significant difference was observed in the corrosion potentials of the three Cu materials (P>0.05). The corrosion current density and corrosion rate of the pure Cu group were significantly higher than those of the Cu-38 Zn and H62 groups (P<0.05). The Cu-38 Zn group showed higher corrosion current density and corrosion rate than the H62 group; however, no significant difference was observed (P>0.05).

3.4. Surface characterization

The long-term corrosion behaviors of pure Cu, Cu-38 Zn, and H62 were determined by immersing the materials in the SUF solutions at 37 $^{\circ}$ C for 300 days. The phase and chemical compositions of the corroded Cu, Cu-38 Zn and H62 were characterized using XRD and XPS spectra, as shown in Fig. 4.

We observed that the pure Cu and Cu alloys corroded as their oxides. Cu_2O was the main crystalline product from pure CU, whereas Cu_2O and ZnO were the main crystallised product from Cu-38 Zn and H62. The peak intensity of Cu_2O increased compared with that of the Cu, with increase in the immersion time. This

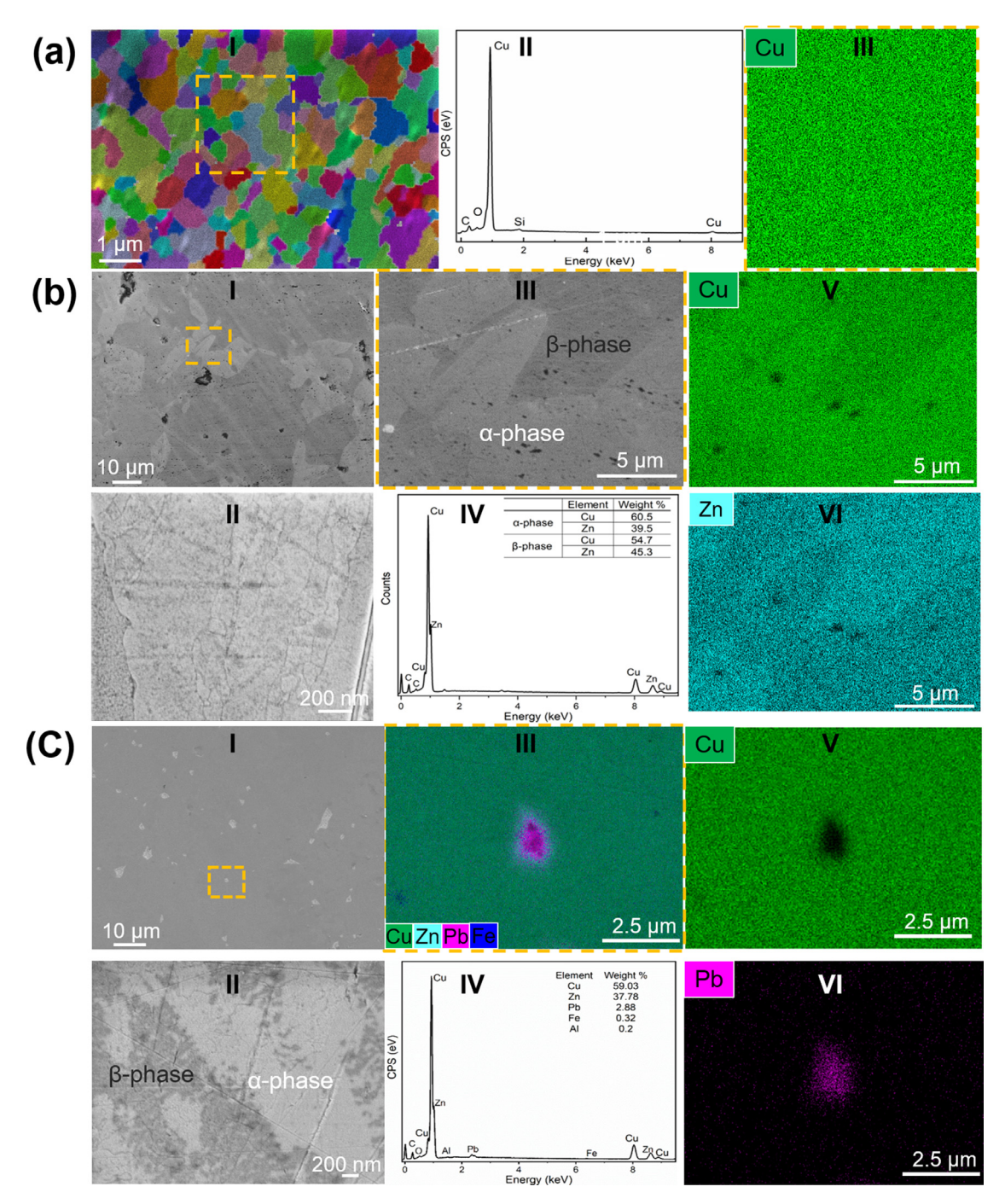


Fig. 1. The microstructures of the pure Cu (a), Cu-38 Zn (b) and H62 (c); a-(I): EBSD image of the Pure Cu showing grains; a-(II): EDX spectrum of the pure Cu corresponding to the squared area in a-(I), a-(III): the Cu elemental mapping of pure Cu corresponding to the squared area in a-(I), b-(I-III): SEM images of the Cu-38 Zn showing phases and grains at different magnifications; b-(IV): EDX spectrum of the Cu-38 Zn in b-(III) corresponding to the squared area in b-(I); b-(V & VI): Cu and Zn elemental mapping of the area of b-(III); c-(I-II): SEM images of the H62 showing phases and grains at low and high magnification; c-(III): is the combined elemental mapping of the squared area in c-(I); c-(IV): EDX spectrum of H62 in c-(III): Cu and Pb elemental mapping of H62 corresponding to c-(III).

result suggested that more Cu_2O was formed. No new corroded products were detected through XRD after long-term immersion.

XPS analysis was performed for Cu materials after 300 days of immersion to obtain the detailed chemical compositions of the corroded products. The XPS results for pure Cu, H62, and Cu-38 Zn are shown in Fig .4b. In the survey spectra of Cu materials, general elements such as Cu, Zn, C, O, P, Cl, and Ca were detected. In the high-resolution spectra of Cu 2p from Cu, H62, and Cu-38 Zn, the peak binding energies of 932.5 eV, 933.8–934 eV, 934.5 eV and 935.8 eV were attributed to Cu/Cu₂O, CuO, Cu(OH)₂, and CuCl₂, re-

spectively [35–37]. The Cu and Cu₂O peaks were difficult to distinguish because of their similar binding energy. Therefore, they were labelled as Cu/Cu₂O. The high-resolution spectra of Ca 2p and P 2p detected from pure Cu, H62, and Cu-38 Zn demonstrated that Ca 2p had two peaks; one peak was between 347.3–347.5 eV $(2p_{3/2})$, which can be assigned as Ca₃(PO₄)₂ [38]. Additionally, the intensity of Ca 2p spectra in the Cu-38 Zn sample was higher that of the H62 sample. Meanwhile, the peak of P 2p detected at 133.3 eV, was consistent with that of the P 2p in Ca₃(PO₄)₂ [39]. In the high-resolution spectra of Zn 2p, the peak binding energy of 1021.8 eV

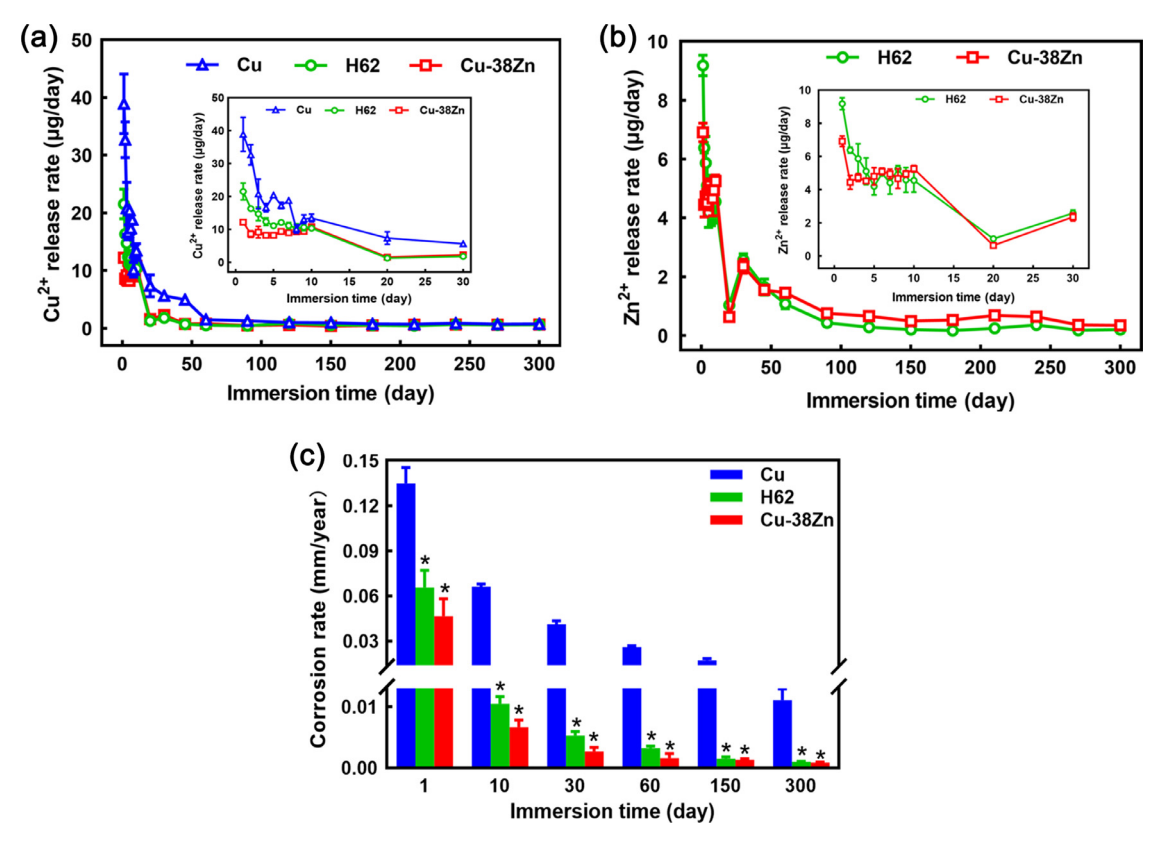


Fig. 2. (a) Cu^2 +release rate of pure Cu, H62, Cu-38 Zn and Zn^2 + release rate of H62, Cu-38 Zn (b) immersed in SUF at 37 °C for 300 days. (c) Corrosion rate values calculated from the weight loss of pure Cu, H62 and Cu-38 Zn after 1, 10, 30, 60, 150 and 300 days of immersion. Line chart represent mean \pm SD, n=5.

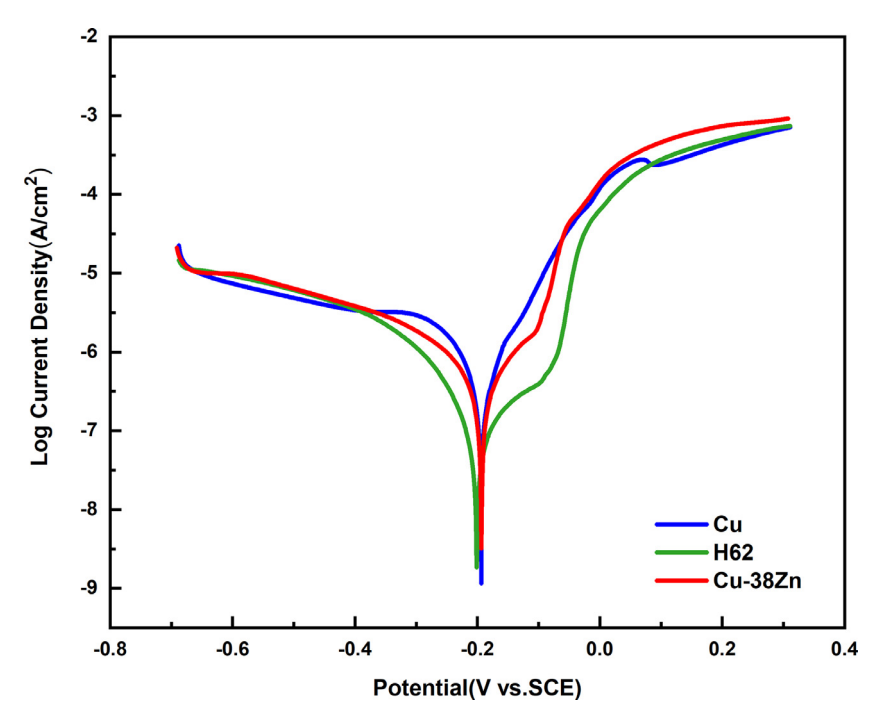


Fig. 3. Potentiodynamic polarization curves of pure Cu, H62 and Cu-38 Zn in SUF with pH values of 7.0.

suggested the existence of Zn (OH) $_2$ [40]. The peak binding energy between 1021.6–1021.9 eV can be characterized as ZnO [41,42]. The peak located at 1022.2–1022.4 eV can be attributed to Zn $_5$ (CO $_3$) $_2$ (OH) $_6$ [40,42]. These compositions were detected through XPS but not by XRD. This finding suggests the presence of low amounts of amorphous phases. The Cu-38 Zn sample exhibited low intensity of

Cu spectra and high intensity of Zn 2p spectra in the SUF solution. By contrast, the H62 sample exhibited high intensity of Cu spectra and low intensity of Zn 2p spectra in the SUF solution.

The morphological changes in the corroded surfaces of Cu, H62, and Cu-38 Zn are shown in Fig. 5. A corroded layer was formed on pure Cu after it was immersed in the SUF solution for one day.

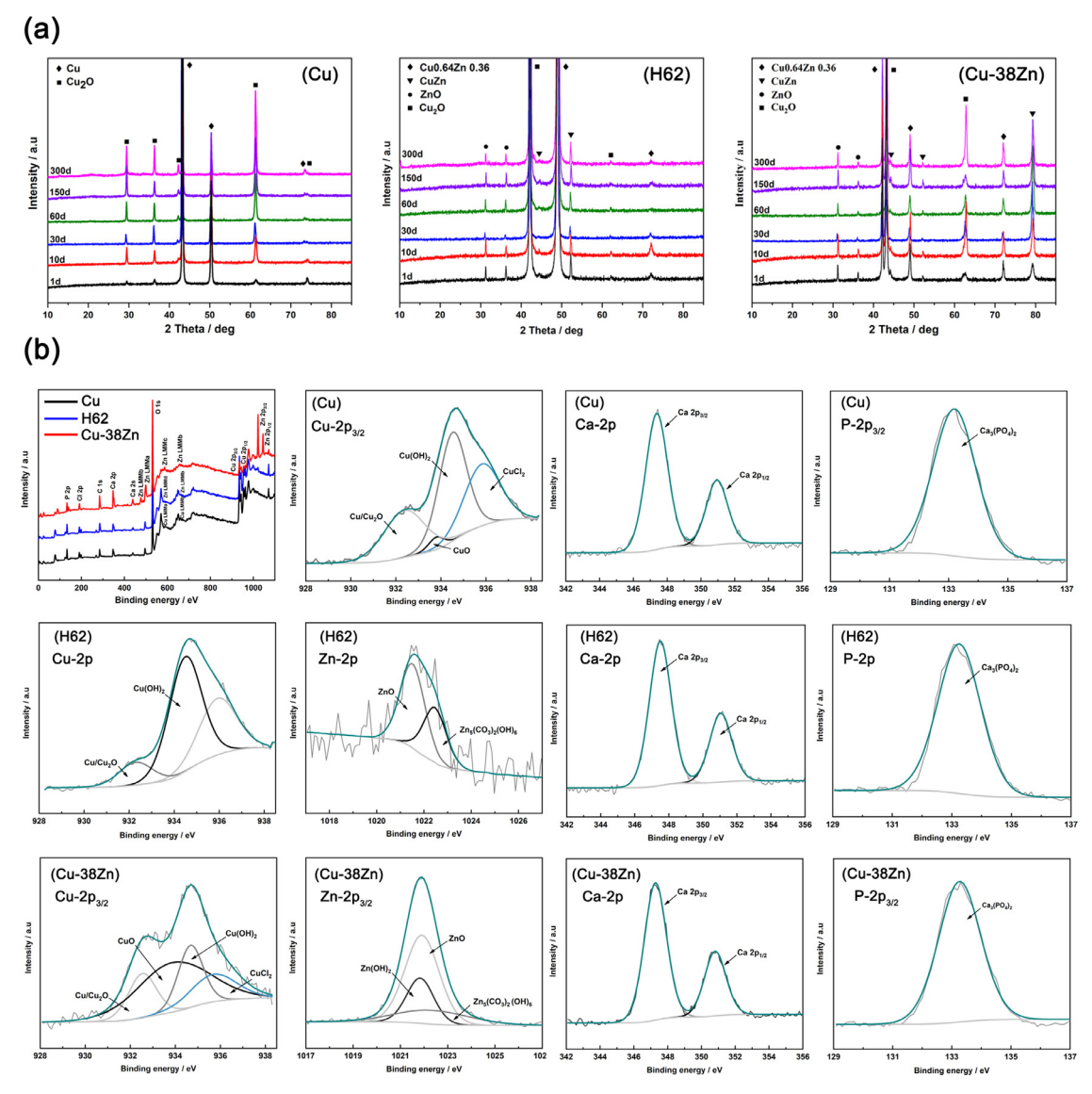


Fig. 4. XRD patterns (a) and XPS spectra (b) of pure Cu, H62 and Cu-38Zn immersed in SUF for different times.

After prolonged immersion for 10 and 30 days, the layer became increasingly dense, with clusters of porous corroded product on the top. The second layer of the fully developed porous clusters was formed after 60 days of immersion. More solid dense clusters were formed as the third corroded layer after 150 and 300 days of immersion. The H62 and Cu-38 Zn sample surfaces were nearly intact after immersion in the SUF solution for one day. Scratches were observed on the surface that was caused by mechanical polishing. After prolonged immersion, a white granular corroded layer was formed on the surfaces. After 60 days of immersion, the white granular corroded laver became thicker, and this laver covered the majority of the H62 sample surface. However, the surface morphology of the Cu-38 Zn sample remained nearly unchanged during the 60 days of immersion. However, as the immersion time prolonged, the number and size of the corroded layer gradually increased. After 300 days of immersion, a compact layer covered the H62 surface, and clusters of white granular corroded product were dispersed on the Cu-38 Zn surface. Cu was found to exhibit a much more obvious color change and corroded surface, followed by H62 and then Cu-38 Zn. As shown in Table 2 and Fig. S2, according to the EDS mapping analysis of surfaces of corroded products, the surface corroded product of the Cu sample was mainly

composed of Cu, C, O, P, Cl, and Ca. The surface corroded product Cu-38 Zn and H62 samples was composed of Cu, Zn, C, O, P, Cl, and Ca. These results are consistent with those of the previous XPS elemental analysis.

3.5. In vitro cytocompatibility analysis

Fig. 6 shows the cell viability measurement results of the 100% extracts from pure Cu and Cu alloys. The viability of HEECs in the 100% extracts of both pure Cu and Cu alloys was extremely low on the first day. In the following days, HEEC viability in the 100% extracts (Fig. 6a) of both pure Cu and H62 exhibited a slight increase. However, the viability of HEECs in the Cu-38 Zn extracts showed an obvious increase. As shown in Fig. 6b, on the first day, the cell viability in the pure Cu 100% extracts was significantly lower than that of the Cu alloys extracts. Unlike HEECs, the HESC viability after day 2 and day 3 in the pure Cu extract increased a bit but reduced markedly Cu alloys extracts. The concentration of ions in the extracts was determined and is presented in Table 3. The concentration of Cu²⁺ was significantly lower in the Cu-38 Zn and H62 extracts than that in the pure Cu extract. The Cu²⁺concentration in the Cu-38 Zn extracts was noticeably less than that in the H62

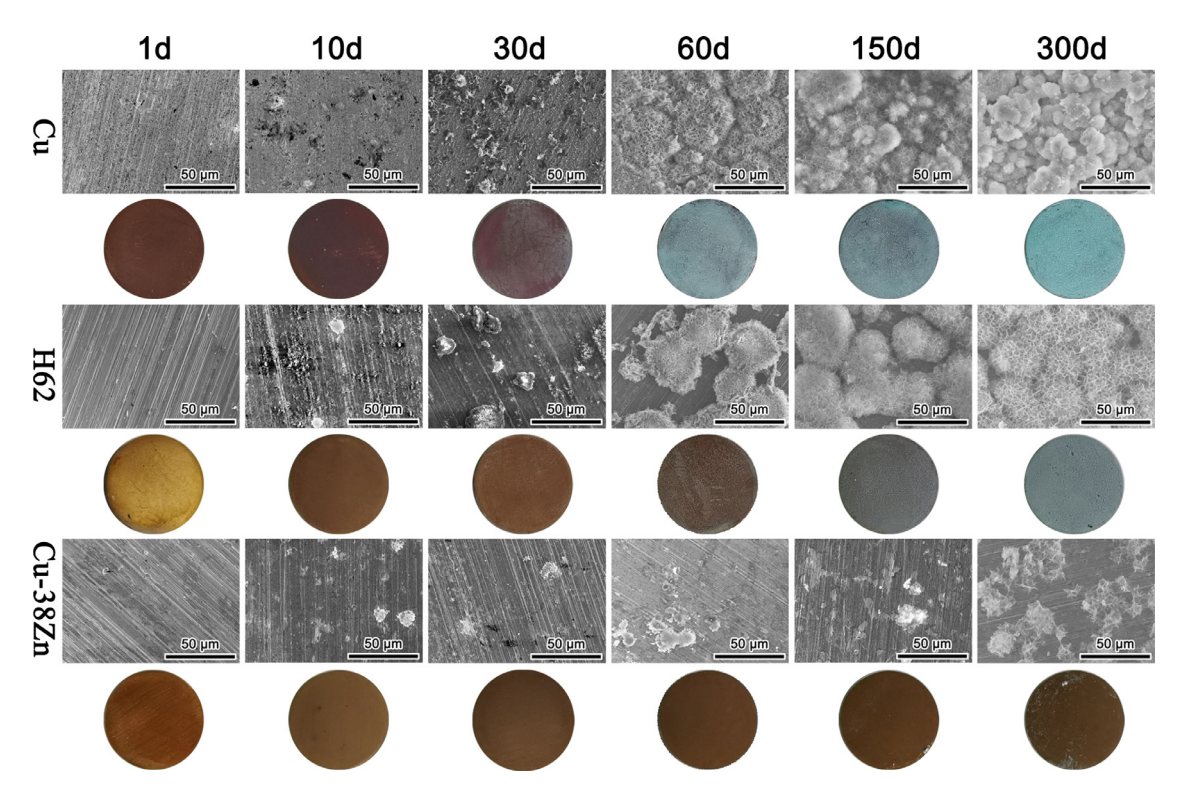


Fig. 5. Surface morphologies of pure Cu, H62 and Cu-38 Zn after immersion in SUF for different times.

Table 2 EDS analysis of pure Cu, H62 and Cu-38 Zn in SUF solutions.

	Cu	Zn	0	С	P	Ca	Cl
Cu sample							
Day 1 – layer	68.82	-	31.18	-	-	-	-
Day 10 -layer	58.26	-	26.66	15.08	-	-	-
Day 10 -porous corrosion product	40.7	-	40.61	7.84	6.87	2.02	1.96
Day 300 -porous corrosion product	15.92	-	54.83	8.23	13.71	4.26	3.04
H62 sample							
Day 1 – layer	51.88	32.88	15.24	-	-	-	-
Day 10 -layer	11.74	17.57	49.07	4.46	11.53	5.63	-
Day 10 -white corrosion product	22.01	8.41	45.60	8.20	10.05	3.59	2.14
Day 300 -white corrosion product	14.11	2.08	53.16	10.74	13.37	3.49	3.05
Cu-38 Zn sample							
Day 1 – layer	56.95	30.30	12.75	-	-	-	-
Day 10 -layer	41.40	19.28	24.04	10.45	2.93	1.89	-
Day 10 -white corrosion product	17.18	7.55	52.96	6.58	10.79	3.31	1.65
Day 300 -layer	34.33	20.11	31.16	8.28	3.39	2.84	-
Day 300 -white corrosion product	13.17	2.95	46.35	22.72	9.85	3.07	1.90

Table 3 Ion concentrations of culture media incubated with pure Cu, H62 and Cu-38 Zn for 24 h. (mean \pm SD; n = 3).

Extracts	DMEM/F12			
	Cu ²⁺ (μg/mL)	Zn ²⁺ (μg/mL)	Fe ²⁺ (μg/mL)	Pb ²⁺ (μg/mL)
Normal Control	0.02±0.01	0.28±0.01	0.25±0.01	_
Pure Cu	130.13±5.63	$0.32 {\pm} 0.02$	1	1
H62	30.96±3.85*	12.19±0.76*	0.26 ± 0.01	$0.30 {\pm} 0.02$
Cu-38Zn	22.64±1.71*	10.86±0.73*	1	1

[&]quot;-" means the absence of this kind of element. "/" means not tested.

extracts. No difference was observed in the Zn^{2+} concentrations of the Cu-38 Zn and H62 extracts. To further determine the effect of Cu^{2+} and Zn^{2+} on cell viability, the cytotoxicity of Cu^{2+} and a mixture of Cu^{2+} and Zn^{2+} on HEECs and HESCs was tested, as shown in Fig. 6c-f. By comparing the toxicity of Cu^{2+} from pure Cu extract with that from the H62 and Cu-38 Zn extracts, we found that the

cell viability increased when the concentration of Cu^{2+} decreased. Meanwhile, cell viability in the Cu^{2+} from the H62 and Cu-38 Zn extract groups was significantly lower than that in the Cu^{2+} and Zn^{2+} mixtures groups. The systemic characterization and comparison suggested that the H62 and Cu-38 Zn samples have better cytocompatibility than the pure Cu sample because of the reduced

^{*} P<0.05 when H62 and Cu-38Zn groups compared to with the pure Cu group.

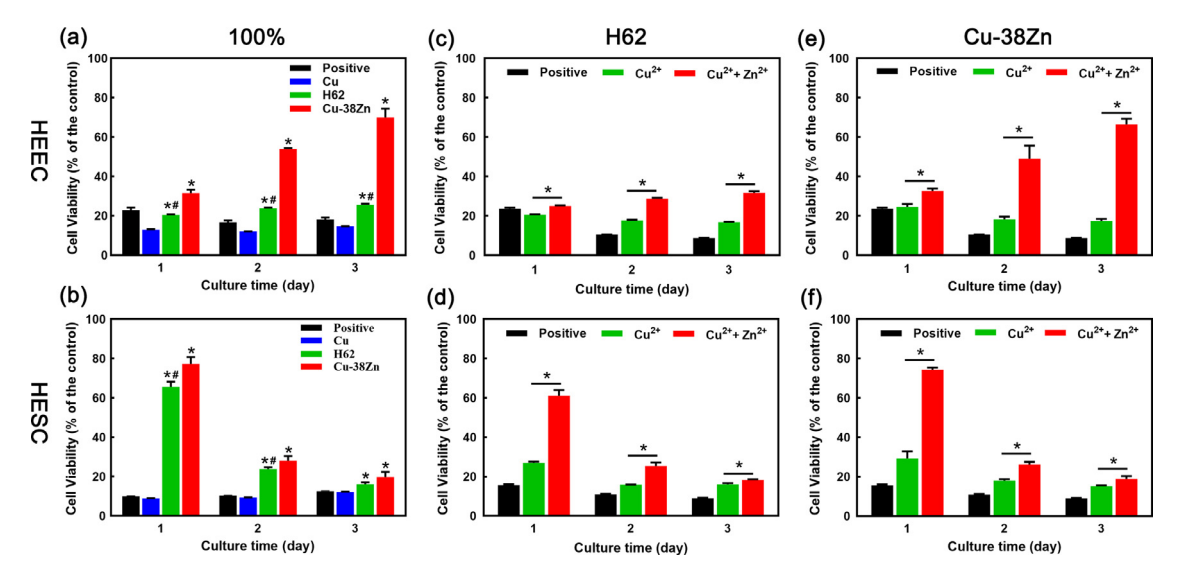


Fig. 6. Viability of HEECs (a) and HESCs (b) cells after 1, 2 and 3days incubation in 100% pure Cu, H62 and Cu-38 Zn extracts. (c, d) viability of HEECs and HESCs at Cu^{2+} and $Cu^{2+} + Zn^{2+}$ concentrations in H62 extracts. (e, f) viability of HEECs and HESCs at Cu^{2+} and $Cu^{2+} + Zn^{2+}$ concentrations in Cu-38 Zn extracts. Data represent mean \pm standard deviation. *P<0.05 when compared with the Cu/Cu²⁺ group, *P<0.05 when H62 group compared with the Cu-38 Zn group.

 ${\rm Cu^{2+}}$ release rate and the antagonistic effect of ${\rm Zn^{2+}}$ on ${\rm Cu^{2+}}$. In addition, no significant difference was observed in the pH of the Cu materials after incubation, as shown in Fig. S3.

3.6. In vivo tests

3.6.1. Histological observations

To evaluate tissue compatibility of the Cu, Cu-38 Zn and H62 materials with the endometrium, we compared the histological changes in the endometrium on days 3, 7, 14, and 28 after the implantation of the materials (Fig. 7). In the SO group at every point, the endometrium epithelial cells and stromal cells were neatly arranged with a clear outline. Complete glandular epithelium and a normal number of glands were observed. Three days after implantation, the endometrial stromal cells were arranged in a disordered manner, in the case of all three materials. Furthermore, the uterine cavity exudated (indicated by black arrowhead) and the uterine luminal epithelial cells disappeared. We also observed bare endometrial lamina propria (indicated by red arrowhead) in the endometrium from the pure Cu and H62 implantation group. This was not observed in the endometrium from the Cu-38 Zn implantation group. Continuous damage was visible in the endometrial tissues 7 days after the pure Cu implantation. We observed an increase in the uterine cavity exudation and shedding of endometrial stromal cells. We also observed cavities in the endometrial stroma of the H62 group, which suggested local edema of the uterine tissue. For the uterine tissue that was in contact with the Cu-38Zn implantation, slight destruction in the endometrium epithelium and stroma structure was observed. After 14 day of pure Cu implantation, the endometrial tissue structure did not improve significantly. Furthermore, we observed large blocks of uterine exudation and endometrial stromal stripping. The uterus tissues that were in contact with the H62 and Cu-38 Zn implantation showed clear signs of repair response, and endometrial stromal cells started to arrange in an orderly manner gradually. Small areas of endometrial epithelium were covered in the H62 group, whereas large areas were covered in the Cu-38 Zn group, after 28 days of implantation, partially recovered endometrial epithelium was observed in the uterus tissues that were in contact with pure Cu. We also observed the disappearance of uterine luminal epithelial cells and the irregular arrangement of endometrial stromal cells.

In the H62 group, we also observed a progressive expansion of endometrial epithelial coverage with well-arranged endometrial stromal cells. The structure of the endometrium and the number of glands were close to normal with well-arranged cells in the Cu-38 Zn group after 28 days of implantation.

3.6.2. Antifertility effectiveness

To determine the contraceptive effect of Cu materials, the antifertility test was carried out in the SD rats; the results are shown in Table 4. Embryos were not observed in the material-bearing uterine horns of the rats, while normal embryos were found in the contralateral uterine horns. The antifertility rate in the material-bearing groups was all 100%, which indicate that Zn addition did not attenuate the antifertility efficacy of Cu materials.

3.6.3. Surface characteristics of the implanted Cu materials

To study the characteristics of surface corrosion on Cu materials after their implantation in the uterine of SD rats for 3, 7, 14, and 28 days, we observed the surface morphologies and extent of corrosion on the implanted Cu materials. As shown in the SEM images (Fig. 8), the surface of pure Cu was severely corroded and some areas were peeling off. Compared with those of the Cu group, the SEM images of the Cu-38 Zn and H62 groups showed relatively smooth surfaces. Minor peeling was observed on the H62 surfaces, whereas no peeling and a much smoother and cleaner surface were observed on Cu-38 Zn.

The chemical compositions of the corroded products of Cu materials after implantation for 28 days were analysed and are shown in Fig. 9. For the pure Cu group, the corroded products were mainly composed of C, N, O, S and Cu. However, the corroded products of the H62 group were composed of C, N, O, S, Cu, P and Zn, and the corroded products of the Cu-38 Zn group were composed of C, N, O, S, Cu, and Zn. Unlike in vitro experiments, N and S were present on the corroded surface of Cu materials implanted in the SD rat uterine cavity. This result indicated that apart from the oxides, some SD rat uterine tissue or organic matter was also deposited on the surface of the Cu materials.

4. Discussion

In the present study, Cu-38 Zn and H62 exhibited better instantaneous and long-term corrosion properties and biocompatibility

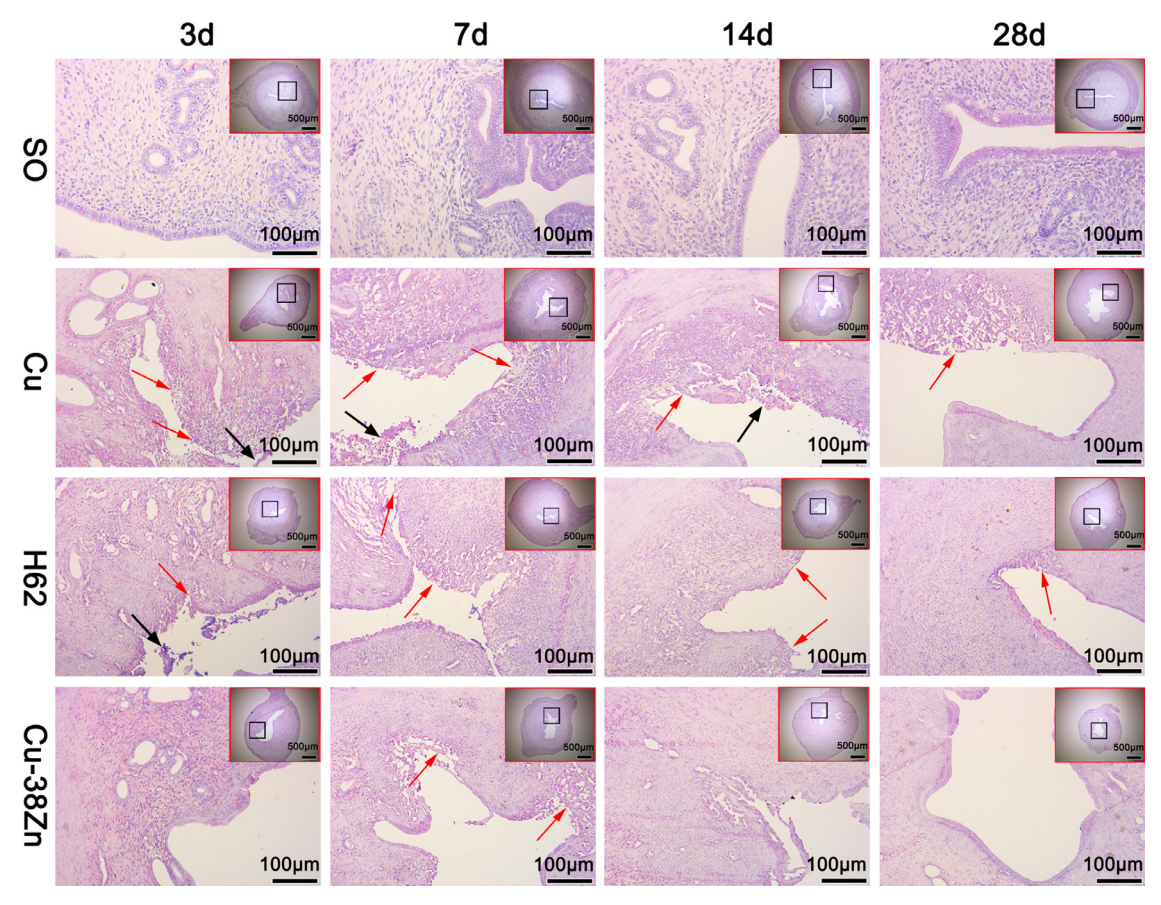


Fig. 7. Histopathology of endometrium in Sprague-Dawley rat after insertion of pure Cu, H62 and Cu-38 Zn for 3, 7, 14 and 28 days. Scale bar = 100 µm.

Table 4
Antifertility effectiveness of pure Cu, H62 and Cu-38 Zn.

Group	n	No. of embryos in material-bearing uterine horn $(\bar{x}\pm SD)$	No. of embryos in contralateral uterine horn $(\bar{x}\pm SD)$	No. of pregnant animals	Antifertility rate (%)
NC	5	7.4 ± 1.4	6.0 ± 1.9	5	0
SO	10	5.3 ± 1.2	4.7 ± 0.9	5	0
Pure Cu	10	0	7.2 ± 1.2	0	100*
H62	10	0	6.4 ± 1.4	0	100*
Cu-38Zn	10	0	5.8 ± 1.5	0	100*

^{*} P<0.05 when compared with the normal control group.

than pure Cu, indicating that Cu-Zn can be considered a potential alternative for the conventional Cu-IUDs.

4.1. Comparison of surface characteristics among Cu materials in vitro and in vivo

The conventional Cu-IUD consists of an inert bracket and a copper wire or sleeve. Copper was oxidized and release soluble corrosion product Cu²⁺ into the uterine cavity to enhance the contraceptive action of Cu-IUDs [4,24]. However, it was found that the corrosion surfaces of Cu materials varied a lot. The insoluble corrosion products adhered to the surface of the corroded Cu materials could induce friction in the interface between Cu materials and endometrium and increase the chance of adverse effects. In other words, the rougher the Cu-IUD surface, the greater is the damage to the endometrium, leading to adverse effects such as cramping, irregular vaginal bleeding, pelvic inflammatory disease, lumbosacral pain [43]. Additionally, some insoluble corrosion products due to peristalsis of the uterine cavity, may be peeling from the Cu materials and eliminated through the cervix of the body. SEM

images analysis of Cu materials used in vitro and in vivo showed that the surface of corroded Cu was rougher than those of the corroded Cu-38 Zn and H62. The results of the electrochemical test and weight loss measurement showed that Cu-38 Zn and H62 exhibited better corrosion resistance than Cu. In addition, the products released by Cu-38 Zn corrosion were lesser in number than those released by Cu and H62 corrosion., and stiff corrosion products might have been involved in incrustation formation and increased the chance of adverse effects [44–46]. In the present study, the surface of corroded Cu-38 Zn was smoother and cleaner than that of the corroded Cu and H62. Cu-38 Zn implants caused lesser damage than the other two implants, indicating that the adverse effects associated with the rough surface can be alleviated.

4.2. Degradation properties of Cu materials in SUF

In this study, SUF was used as the corrosion media to investigate the corrosion behaviors of Cu materials. A schematic illustration of the corrosion process involved is presented in Fig. 10.

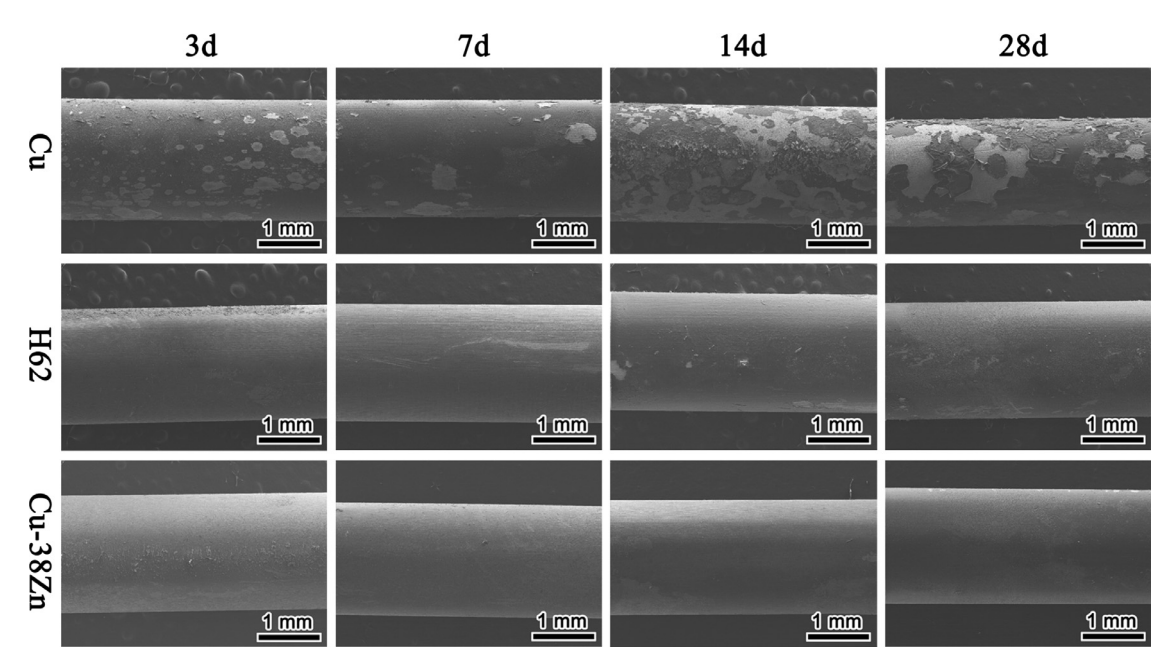


Fig. 8. SEM images of pure Cu, H62 and Cu-38 Zn after implantation for 3, 7, 14 and 28 days.

The corrosion process of copper in SUF has been studied previously [47,48]. The reactions taking place during copper corrosion in SUF are given as Eqs. (1) and (2).

$$8Cu + 2H_2O + O_2 \rightarrow 4Cu_2O + 4H^+ + 4e^-$$
 (1)

$$Cu_2O + 2H^+ \rightarrow 2Cu^{2+} + H_2O + e^-$$
 (2)

 Cu_2O is thermodynamically unstable and is easily oxidised into Cu^{2+} [49,50]. As immersion time in SUF progresses, redox transformations occur from Cu_2O to cupric oxide (CuO) or Cu (OH)₂ occurred (Eqs. (3) and 4) [51].

$$Cu_2O + H_2O \rightarrow 2CuO + 2H^+ + 2e^-$$
 (3)

$$Cu_2O + 2H_2O \rightarrow 2Cu (OH)_2 + 2H^+ + 2e^-$$
 (4)

The optical micrograph and XRD results (Fig. 1 and Fig. 5) showed that Cu-38 Zn alloy contains Cu matrix and Cu-Zn intermetallic phases unlike pure copper. Consequently, Cu and Zn were corroded (Eqs. (1),2, and 5), accompanied by the reduction of oxygen as the cathodic reaction (Eq. (6)). Copper corrosion resulted in the formation of a Cu₂O film on the alloy surface. In addition, the increased levels of Zn²⁺ and OH⁻ promoted the generation of Zn (OH)₂ (Eq. (7)), followed by transformation into ZnO (Eq. (8)) [52]. The presence of Zn₅(CO₃)₂(OH)₆ on Cu-38 Zn surface, as described in Eq. (9), was confirmed by XPS analysis. Other studies have reported Zn₅(CO₃)₂(OH)₆ as the corrosion product of zinc formed in the presence of NaCl and simulated body fluid solutions [53,54].

$$Zn \rightarrow Zn^{2+} + 2e^{-} \tag{5}$$

$$O_2 + 2H_2O + 4e^- \rightarrow 4OH^-$$
 (6)

$$Zn^{2+} + 2OH^{-} \rightarrow Zn (OH)_{2}$$
 (7)

$$Zn (OH)_2 \rightarrow ZnO + H_2O \tag{8}$$

$$5Zn^{2+} + 2HCO-3 + 8OH^{-} \rightarrow Zn_{5}(CO_{3})_{2}(OH)_{6} + 2H_{2}O$$
 (9)

$$Zn (OH)_2 + 2Cl^- \rightarrow Zn^{2+} + 2OH^- + 2Cl^-$$
 (10)

$$3Ca^{2+} + 2PO3 - 4 \rightarrow Ca_3(PO_4)_2$$
 (11)

Three types of anions are present in SUF: chlorine, bicarbonate, and dihydrogen phosphate ions. Chlorine ions attack the hydroxide group, as described in Eq. (10) [55]. Moreover, $Ca_3(PO_4)_2$ was formed on the surface of Cu materials (Eq. (11)). It is generally accepted that the alkalization of the solution could promote the generation of $Ca_3(PO_4)_2$ [56]. In the present study, increased pH values were observed in SUF after 300 days of immersion (Fig. S4), which favored the formation of $Ca_3(PO_4)_2$.

The corrosion rates were determined 28 days after implantation, and the pure Cu, H62 alloy and Cu-38 Zn alloy implants exhibited corrosion rates of 0.055 mm/y, 0.008 mm/y, and 0.007 mm/y, respectively. The corrosion rates observed in-vivo implantation into the uterine cavity were higher than those observed in the in-vitro immersion tests. Previously, when Cu was used as the implanted material, its corrosion rate was accelerated because of the presence of organic components in the uterine fluid such as serum albumin and fibrinogen [57]. Another cause of the difference in corrosion between the in vivo and in vitro results could be different hydrodynamic conditions affecting the implant surface [58]. Therefore, the uterine environment might have accelerated the corrosion process of Cu materials in the present study.

4.3. Biocompatibility of Cu materials in-vitro and in-vivo studies

Adverse effects of the conventional Cu-IUD, such as irregular bleeding and pain have not been resolved in clinical practice. It is believed that the occurrence of these adverse effects is associated with the initial burst release of Cu^{2+} [47]. Many studies have reported the initial burst release of Cu^{2+} in vitro [7,8,16–21,47,59–69]. The comparison between the results of the present study and those of previous in-vitro studies on Cu^{2+} release from Cu-IUDs and bulk copper materials in SUF is presented in Table S5. Briefly, some differences exist in the burst release of Cu^{2+} under different SUF conditions. The maximum Cu^{2+} release rate of pure Cu in the present study was 38.91 μ g/day. However, the Cu-38 Zn group showed more than 60% reduction in the initial burst release of Cu^{2+} than that in the pure Cu group, indicating that the Cu-IUDs prepared from Cu-38 Zn materials could alleviate the adverse effects resulting from the initial burst release of Cu^{2+} . In the later

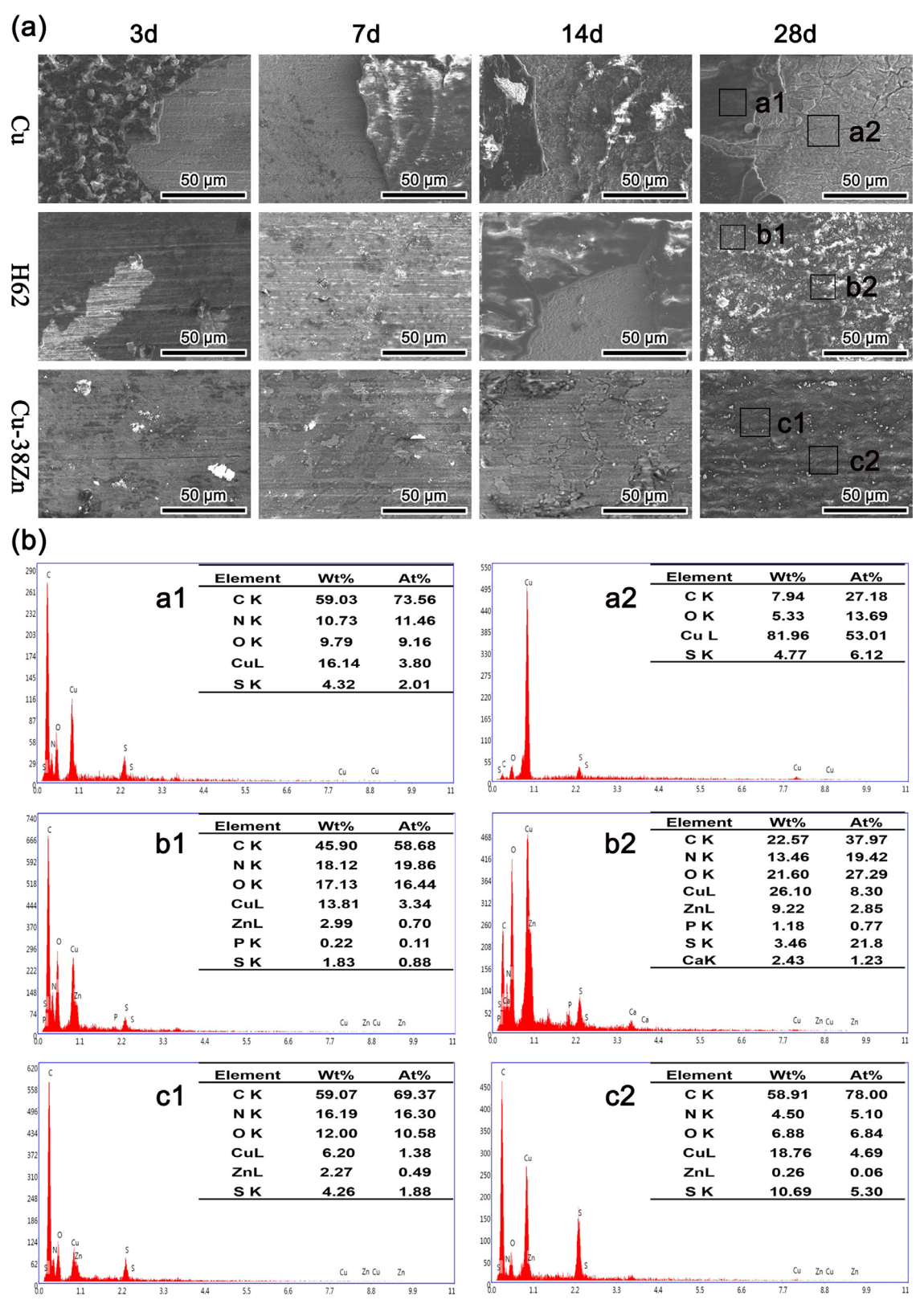


Fig. 9. EDS analysis of pure Cu, H62 and Cu-38 Zn after implantation for 3, 7, 14 and 28 days.

stage, Cu²⁺ release rates of Cu materials decreased slowly with immersion time. The comparison of corrosion properties among the materials showed that the Cu-38 Zn alloy exhibited better instantaneous and long-term corrosion properties than pure Cu, derived from the different metal activities. The metal activity of Zn was

stronger than that of Cu. A large amount of Zn in the Cu-38 Zn alloy can form a galvanic cell with Cu, thereby inhibiting the corrosion of Cu and reducing the Cu^{2+} release. In addition, the corrosion of Zn in the uterine cavity involves the formation of a ZnO protective layer, which can further improve the corrosion resistance

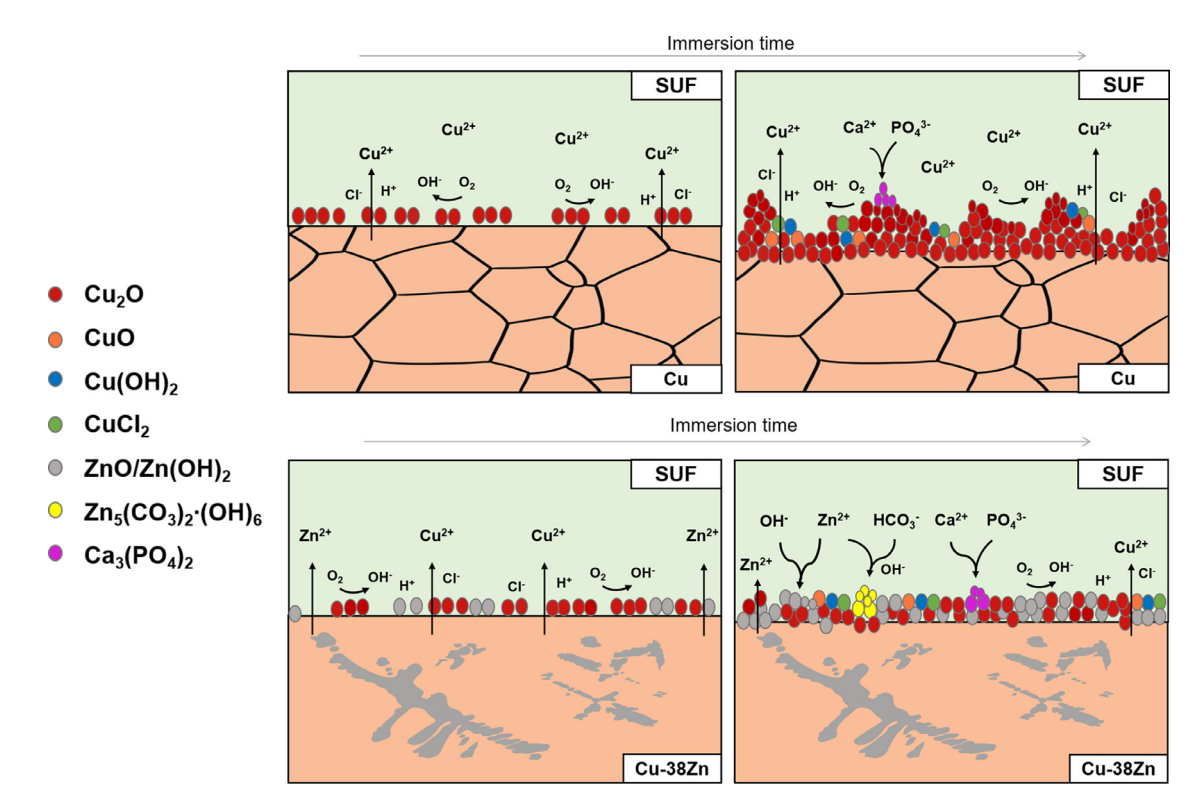


Fig. 10. Schematic illustration of the corrosion behavior of (a) pure Cu and (b) Cu-38 Zn in SUF.

of Cu-38 Zn alloy and reduce the release of ions in the initial and sustained release. Liang et al. [7] reported the Cu²⁺ release rates of TCu380A in SUF to be $0.55 \pm 0.12 \mu g/day$ from day 50 to 250. Additionally, Bastidas [67] reported that the release rate of Cu²⁺ from copper was 0.1 - 0.3 µg/day at 360 days. In the present study, Cu²⁺ release from pure Cu, Cu-38 Zn, and H62 was approximately 1.69-, 1.09- and 1.24-fold higher than that reported by Liang, and approximately 3.1-, 2.27- and 2-fold higher than the maximum release reported by Bastidas. Hagenfeldt et al. [70] measured the concentrations of copper in the uterine fluid from women by using the Cu-T200 device for intrauterine contraception. The copper concentrations in the uterine washing fluid (2 mL) in the proliferative and secretory phases during the 6th - 7th menstrual cycle were 0.31 μg/mL and 0.29 μg/mL, respectively. Specifically, Cu²⁺ release from pure Cu and Cu-38 Zn was 1.5 - 1.60 and 1.1 - 1.17 times higher than that reported by Hagenfeldt, respectively, whereas that from H62 was within the reported range. These results suggested that Cu^{2+} release from pure Cu, Cu-38 Zn, and H62 is sufficient for

Cu-IUDs vary in corrosion process for their different characteristics. It is reported [8] that Cu²⁺ release was mainly controlled by frame, copper type (disk, wire, sleeve) and indomethacin while the shape variation had little influence on Cu²⁺ release. Besides, the effect of copper surface area was only noticeable during the first month. In our report, we simplified the Cu materials and cut them into disks and measured, compared their corrosive performance under the same environment. The exposed surface areas of the Cu materials were normalized to the wires in the typical IUD220. In the further studies, we will continue to investigate the influence of device characteristics on Cu material corrosion process in the uterine environment.

Cu²⁺ plays a crucial role in the contraceptive mechanism of Cu-IUDs [71]. It stimulates an inflammatory response or foreign body reaction, which exhibits spermicidal effect, impedes ovum development, and inhibits embryo implantation after fertilization

[72,73]. However, the cytotoxicity of Cu^{2+} is significant at a higher concentration [64]. Furthermore, exposure to higher concentration of Cu2+ can lead to changes in biochemical factors and endometrium morphology, which may result in undesirable adverse effects [15,74]. Wu et al. [27] reported that 50% toxic concentration of Cu^{2+} to HEECs is 170 μ M (10.80 μ g/mL) at 24 h of incubation. In the present study, we evaluated the effects of Cu material extracts on cell viability, The supernatant is collected and centrifuged to prepare the extract, mainly considering the effect of copper and zinc ions released in the extract on the cytotoxicity. It is found that pure Cu exhibited significant cytotoxicity to HEECs and HESCs (cell viability lower than 20%), as shown in Fig. 6. By contrast, cell viability was dramatically increased when Cu-38 Zn and H62 extracts were used. It suggested that the concentration of Cu²⁺ released by Cu-38 Zn and H62 extracts media was significantly less than that released by Cu extracts. On the other hand, the Cu^{2+} of Cu-38 Zn and H62 alloy materials in combination with Zn²⁺ exhibited antagonistic effect on cytotoxicity against HEECs and HESCs. In addition, the results showed that cell viability was significantly higher in the presence of Cu-38 Zn extracts than that the presence of in H62 extracts. It may be because of the impurities present (Pb and Fe) in the commercial H62 sample that might have inhibited cell viability. At the cellular scale, Pb ions disrupts the energy state of cells, causing ultrastructural and functional disorders in mitochondrial metabolism by decreasing mitochondrial membrane potential, depleting adenosine triphosphate (ATP) pool, and increasing the production of reactive oxygen species [75]. Moreover, Pb influences the expression of mRNAs in the immediate early genes fos and jun [76-77], inhibits DNA repair, and exerts indirect genotoxic effects by acting as a co-mutagen [78]. Cu²⁺ in combination with Zn²⁺exhibited a significant bimodal antagonistic cytotoxicity effect on HEECs when the Cu²⁺ concentration ranged between 200 and $500\,\mu\text{M}$ (12.7 - $31.75\,\mu\text{g/mL}$) and Zn^{2+} concentration ranged between 50 and 150 μ M (3.25 - 9.75 μ g/mL) [27]. The Cu²⁺+Zn²⁺ system of Cu-38 Zn exhibited stronger antagonistic effect than that

of H62. Therefore, Cu^{2+} and Zn^{2+} released from Cu-38 Zn exhibited a better cellular response than those from Cu and H62.

The soluble and insoluble corrosion products are formed in vivo implantation, which produce different effect respectively. Histological observation in the endometrium showed that the Cu-38 Zn exhibited relatively better compatibility than pure Cu and H62. Furthermore, the integrity of the endometrial structure was recovered in the Cu-38 Zn group after 28 days of observation. However, obvious damage to the endometrium structure was observed in the Cu and H62 groups after 14-day and 28-day implantation. All these results showed that the Cu-38 Zn material exhibits good biocompatibility, corrosion resistance, and satisfactory contraceptive efficacy.

5. Conclusion

In this study, Cu-38 Zn alloy was developed as an active metal material for use in IUDs. Corrosion performance, biocompatibility, and contraceptive efficacy of Cu-38 Zn alloy were systematically studied, and main findings are as follows:

- (1) Compared with pure Cu and H62, Cu-38 Zn exhibited markedly reduced burst release of Cu²⁺ in the first few days of the in vitro immersion test.
- (2) Compared with pure Cu and H62, Cu-38 Zn induced less cytotoxicity to the uterine cells (HEECs and HESCs) in vitro.
- (3) Histopathological observations of the endometrium showed that Cu-38 Zn induced less endometrium tissue damage and shorter recovery period compared with pure Cu and H62 and that the surface of Cu-38 Zn was smoother than that of pure and H62.
- (4) The contraceptive efficacy of Cu-38 Zn and H62 is comparable to that of pure Cu.
- (5) Cu-38 Zn alloy exhibited better biocompatibility than the pure Cu and H62, and therefore, it might be considered a promising candidate for developing IUDs.

Declaration of Competing Interest

The authors declare that they have no known competing financial interests or personal relationships that could have appeared to influence the work reported in this paper.

Acknowledgements

This work was supported by the National Key R&D Program of China (Grant No.2016YFC1000903), the Non-profit Central Research Institute Fund of National Research Institute For Family Planning (Grant No. 2020GJZ07), CAMS Innovation Fund for Medical Sciences (CIFMS) (Grant No.2018-I2M-1–004), and National Natural Science Foundation of China (Grant No. 51931001).

Supplementary materials

Supplementary material associated with this article can be found, in the online version, at doi:10.1016/j.actbio.2021.11.006.

References

- [1] J.K.R. Francis, M.A. Gold, Long-Acting Reversible Contraception for Adolescents: a Review, JAMA Pediatr. 171 (7) (2017) 694–701.
- [2] E.C.W. Group, Intrauterine devices and intrauterine systems, Hum. Reprod. Update 14 (3) (2008) 197–208.
- [3] E. Colli, D. Tong, R. Penhallegon, F. Parazzini, Reasons for contraceptive discontinuation in women 20-39 years old in New Zealand, Contraception 59 (4) (1999) 227–231.
- [4] H. Timonen, Copper release from Copper-T intrauterine devices, Contraception 14 (1) (1976) 25–38.
- [5] I. Batar, A. Kuukankorpi, M. Siljander, K. Elomaa, I. Rauramo, Five-year clinical experiences with NOVA T 380 copper IUD, Contraception 66 (5) (2002) 309–314

[6] J. Stanback, D. Grimes, Can intrauterine device removals for bleeding or pain be predicted at a one-month follow-up visit? a multivariate analysis, Contraception 58 (6) (1998) 357–360.

- [7] L. Jinying, L. Ying, G. Xuan, G. Yanli, L. Jianping, Investigation of the release behavior of cupric ion for three types of Cu-IUDs and indomethacin for medicated Cu-IUD in simulated uterine fluid, Contraception 77 (4) (2008) 299–302.
- [8] S. Zhang, Y. Li, P. Yu, T. Chen, W. Zhou, W. Zhang, J. Liu, In vitro release of cupric ion from intrauterine devices: influence of frame, shape, copper surface area and indomethacin, Biomed. Microdevices 17 (1) (2015) 19.
- [9] F. Alvarez, P.L. Schilardi, M.F. de Mele, Reduction of the "burst release" of copper ions from copper-based intrauterine devices by organic inhibitors, Contraception 85 (1) (2012) 91–98.
- [10] K. Patai, G. Szilagyi, B. Noszal, I. Szentmariay, Local tissue effects of coppercontaining intrauterine devices, Fertil. Steril. 80 (5) (2003) 1281–1283.
- [11] G. Farr, R. Amatya, Contraceptive efficacy of the Copper T 380A and Copper T 200 intrauterine devices: results from a comparative clinical trial in six developing countries, Contraception 49 (3) (1994) 231–243.
- [12] P.A. O'Brien, R. Kulier, F.M. Helmerhorst, M. Usher-Patel, C. d'Arcangues, Copper-containing, framed intrauterine devices for contraception: a systematic review of randomized controlled trials, Contraception 77 (5) (2008) 318–327.
- [13] D.A. Grimes, D. Hubacher, L.M. Lopez, K.F. Schulz, Non-steroidal anti-inflammatory drugs for heavy bleeding or pain associated with intrauterine-device use, Cochrane Database Syst. Rev. (4) (2006) CD006034.
- [14] D.A. Grimes, L.M. Lopez, C. Manion, K.F. Schulz, Cochrane systematic reviews of IUD trials: lessons learned, Contraception 75 (6 Suppl) (2007) S55–S59.
- [15] X. Xia, C. Xie, Y. Wang, S. Cai, C. Zhu, X. Yang, The forces imposed by the novel T-shape Cu/LDPE nanocomposite intrauterine devices on the simulated uterine cavity, Contraception 76 (4) (2007) 326–330.
- [16] T. Xu, H. Lei, S.Z. Cai, X.P. Xia, C.S. Xie, The release of cupric ion in simulated uterine: new material nano-Cu/low-density polyethylene used for intrauterine devices, Contraception 70 (2) (2004) 153–157.
- [17] S. Cai, X. Xia, C. Xie, Corrosion behavior of copper/LDPE nanocomposites in simulated uterine solution, Biomaterials 26 (15) (2005) 2671–2676.
- [18] J. Li, J. Suo, X. Huang, C. Ye, X. Wu, Comparison of the release behaviors of cupric ions from metallic copper and a novel composite in simulated body fluid, J. Biomed. Mater. Res. B Appl. Biomater. 85 (1) (2008) 172–179.
- [19] J. Li, J. Suo, X. Huang, L. Jia, Study on a novel copper-containing composite for contraception, Contraception 79 (6) (2009) 439–444.
- [20] J. Li, J. Suo, X. Huang, C. Ye, X. Wu, Release behavior of copper ion in a novel contraceptive composite, Contraception 76 (3) (2007) 233–237.
- [21] X. Xia, Y. Wang, S. Cai, C. Xie, C. Zhu, Will ethylene oxide sterilization influence the application of novel Cu/LDPE nanocomposite intrauterine devices? Contraception 79 (1) (2009) 65–70.
- [22] M. Ahmed, G. Punshon, A. Darbyshire, A.M. Seifalian, Effects of sterilization treatments on bulk and surface properties of nanocomposite biomaterials, J. Biomed. Mater. Res. B Appl. Biomater. 101 (7) (2013) 1182–1190.
- [23] K.M. Hambidge, N.F. Krebs, Zinc deficiency: a special challenge, J. Nutr. 137 (4) (2007) 1101–1105.
- [24] J. Zipper, M. Medel, R. Prager, Suppression of fertility by intrauterine copper and zinc in rabbits. A new approach to intrauterine contraception, Am. J. Obstet. Gynecol. 105 (4) (1969) 529–534.
- [25] P.H. Lin, M. Sermersheim, H. Li, P.H.U. Lee, S.M. Steinberg, J. Ma, Zinc in Wound Healing Modulation, Nutrients 10 (1) (2017).
- [26] P.W. Osinaga, R.H. Grande, R.Y. Ballester, M.R. Simionato, C.R. Delgado Rodrigues, A. Muench, Zinc sulfate addition to glass-ionomer-based cements: influence on physical and antibacterial properties, zinc and fluoride release, Dent. Mater. 19 (3) (2003) 212–217.
- [27] J. Wu, L. Wang, J. He, C. Zhu, In vitro cytotoxicity of Cu2+, Zn2+, Ag+and their mixtures on primary human endometrial epithelial cells, Contraception 85 (5) (2012) 509-518.
- [28] ASTM G1-03-E Standard Practice For Preparing, Cleaning, and Evaluating Corrosion Test Specimens, ASTM International, Philadelphia West Conshohocken, PA, 2014.
- [29] ISO 10993-12:2012 Biological evaluation of Medical Devices-Part 12: Sample preparation and Reference Materials, 2012 https://www.iso.org/standard/53468.html.
- [30] Q.B. Fan, Guo, Dongfeng Ge, Kun Wang, Mingming Sun, Tingting Liu, Jianing Liu, Zechuan Zhang, Xiangbo Xu, Xiaoxue Xu, Bin He, Jiancun Rao, Yufeng Zheng, Effective easing of the side effects of copper intrauterine devices using ultra-fine-grained Cu-0.4Mg alloy, Acta Biomater. 128 (2021) 523–539.
- [31] Y. W, S. Hu, D. Ke, F. Zhou, G. Cheng, W. Xia, C. Zhu, Antifertility effectiveness of a novel copper-containing intrauterine device material and its influence on the endometrial environment in rats, Mater. Sci. Eng. C Mater. Biol. Appl. 89 (2018) 444–455.
- [32] S. H, X. Peng, T. Meng, J. Suo, C. Xiong, The antifertility effectiveness of a novel copper-containing composite used in intrauterine contraceptive devices and the releasing behavior of cupric ions contained in the composite in rats, Contraception 86 (2012) 413–418.
- [33] G. Pantazopoulos, A. Vazdirvanidis, Characterization of the Microstructural Aspects of Machinable α - β Phase Brass, Microsc. Anal. 22 (5) (2008).
- [34] H.L. Hong, Q. Wang, C. Dong, P.K. Liaw, Understanding the Cu-Zn brass alloys using a short-range-order cluster model: significance of specific compositions of industrial alloys, Sci. Rep. 4 (2014) 7065.
- [35] N.S. McIntyre, M.G. Cook, X-ray photoelectron studies on some oxides and hydroxides of cobalt, nickel, and copper, Anal. Chem. 47 (13) (2002) 2208–2213.

- [36] C.D. Wagner, J.F. Moulder, L.E. Davis, Handbook of X-ray Photoelectron Spectrascopy, Perkin-Elmer Corp, 1992.
- [37] T. Jin, W. Zhang, N. Li, X. Liu, L. Han, W. Dai, Surface Characterization and Corrosion Behavior of 90/10 Copper-Nickel Alloy in Marine Environment, Materials (Basel) 12 (11) (2019).
- [38] T. Hanawa, S. Hiromoto, K. Asami, Characterization of the surface oxide film of a Co-Cr-Mo alloy after being located in quasi-biological environments using XPS, Appl. Surf. Sci. 183 (2001).
- [39] S. Champagne, E. Mostaed, F. Safizadeh, E. Ghali, M. Vedani, H. Hermawan, In Vitro Degradation of Absorbable Zinc Alloys in Artificial Urine, Materials (Basel) 12 (2) (2019).
- [40] G. Ballerini, K. Ogle, M.G. Barthés-Labrousse, The acid-base properties of the surface of native zinc oxide layers: an XPS study of adsorption of 1,2-diaminoethane, Appl. Surf. Sci. 253 (16) (2007) 6860-6867.
- aminoethane, Appl. Surf. Sci. 253 (16) (2007) 6860–6867.
 [41] G. Katarivas Levy, A. Kafri, Y. Ventura, A. Leon, R. Vago, J. Goldman, E. Aghion, Surface stabilization treatment enhances initial cell viability and adhesion for biodegradable zinc alloys, Mater. Lett. 248 (2019) 130–133.
- [42] L.S. Dake, D.R. Baer, J.M. Zachara, Auger parameter measurements of zinc-compounds relevant to zinc transport in the environment, Surf. Interface Anal. 14 (1989)
- [43] X. Xia, C. Xie, C. Zhu, S. Cai, X. Yang, Effect of implanted Cu/low-density polyethylene nanocomposite on the morphology of endometrium in the mouse, Fertil. Steril. 88 (2) (2007) 472–478.
- [44] K. Patai, M. Berenyi, M. Sipos, B. Noszal, Characterization of calcified deposits on contraceptive intrauterine devices, Contraception 58 (5) (1998) 305–308.
- [45] M. Rizk, N. Shaban, I. Medhat, Y. Moby el Dien, M.A. Ollo, Electron microscopic and chemical study of the deposits formed on the copper and inert IUCDs, Contraception 42 (6) (1990) 643–653.
- [46] J.M. Bastidas, N. Mora, E. Cano, J.L. Polo, Characterization of copper corrosion products originated in simulated uterine fluids and on packaged intrauterine devices, J. Mater. Sci. Mater. Med. 12 (5) (2001) 391–397.
- [47] C. Zhang, N. Xu, B. Yang, The corrosion behaviour of copper in simulated uterine fluid, Corros. Sci. 38 (4) (1996) 635–641.
- [48] H. Xue, N. Xu, C. Zhang, Corrosion behavior of copper in a copper bearing intrauterine device in the presence of indomethacin, Contraception 57 (1) (1998) 49–53
- [49] S.A. Campbell, G.J.W. Radford, C.D.S. Tuck, B.D. Barker, Corrosion and galvanic compatibility studies of a high-strength copper–nickel alloy, Corrosion 58 (2002).
- [50] R. Babic, M. Metikos-Hukovic, M. Loncıı̃ar, Impedance and photoelectrochemical study of surface layers on Cu and Cu-10Ni in acetate solution containing benzotriazole, Electrochim. Acta 44 (1999).
- [51] A.L. Ma, S.L. Jiang, Y.G. Zheng, W. Ke, Corrosion product film formed on the 90/10 copper–nickel tube in natural seawater: composition/structure and formation mechanism, Corros. Sci. 91 (2015) 245–261.
- [52] H. Yang, X. Qu, W. Lin, D. Chen, D. Zhu, K. Dai, Y. Zheng, Enhanced Osseointe-gration of Zn-Mg Composites by Tuning the Release of Zn Ions with Sacrificial Mg-Rich Anode Design, ACS Biomater. Sci. Eng. 5 (2) (2018) 453–467.
- [53] X. Liu, Y. Cheng, Z. Guan, Y. Zheng, Exploring the effect of amino acid and glucose on the biodegradation of pure Zn, Corros. Sci. 170 (2020).
- [54] L. Xiao, Y. Hongtao, X. Pan, Comparative studies of Tris-HCl, HEPES and NaHCO3/CO2 buffer systems on the biodegradation behaviour of pure Zn in NaCl and SBF solutions, Corros. Sci. 157 (2019).
- [55] J. Venezuela, M.S. Dargusch, The influence of alloying and fabrication techniques on the mechanical properties, biodegradability and biocompatibility of zinc: a comprehensive review, Acta Biomater. 87 (2019) 1–40.
- [56] S. Naddaf Dezfuli, Z. Huan, J.M.C. Mol, M.A. Leeflang, J. Chang, J. Zhou, Influence of HEPES buffer on the local pH and formation of surface layer during in vitro degradation tests of magnesium in DMEM, Prog. Nat. Sci.: Mater. Int. 24 (5) (2014) 531–538.

- [57] G.C. Clark, D.F. Williams, The effects of proteins on metallic corrosion, J. Biomed. Mater. Res. 16 (2) (1982) 125–134.
- [58] N. Eliaz, Corrosion of Metallic Biomaterials: a Review, Materials (Basel) 12 (3) (2019).
- [59] R. Ramakrishnan, B. B, A.S. Aprem, Controlled release of copper from an intrauterine device using a biodegradable polymer, Contraception 92 (6) (2015) 585–588.
- [60] B. Cao, T. Xi, Y. Zheng, Release behavior of cupric ions for TCu380A and TCu220C IUDs, Biomed. Mater. 3 (4) (2008) 044114.
- [61] X. Zhou, Y. Li, X. Jiang, L. Qiu, J. Liu, Release of copper and indomethacin from intrauterine devices immersed in simulated uterine fluid, Eur. J. Contracept. Reprod. Health Care 15 (3) (2010) 205–212.
- [62] J. Gao, Y. Li, J.-p. Liu, X. Gu, Releasing of Cupric Ion of Three types of Copper-bearing Intrauterine Contraceptive Device in Simulated Uterine Fluid, J. Reprod. Contraception 18 (1) (2007) 33–40.
- [63] Z. Yang, C. Xie, S. Cai, X. Xia, Effects of LDPE film on the properties of copper/LDPE composites for intrauterine contraceptive device, Mater. Lett. 62 (26) (2008) 4226–4228.
- [64] X.X. Xu, M.H. Ding, J.X. Zhang, W. Zheng, L. Li, Y.F. Zheng, A novel copper/polydimethiylsiloxane nanocomposite for copper-containing intrauterine contraceptive devices, J. Biomed. Mater. Res. B Appl. Biomater. 101 (8) (2013) 1428–1436.
- [65] C. Qi, X. Xia, W. Zhang, C. Xie, S. Cai, Indomethacin/Cu/LDPE porous composite for medicated copper intrauterine devices with controlled release performances, Compos. Sci. Technol. 72 (3) (2012) 428–434.
- [66] W. Zhang, X. Xia, C. Qi, C. Xie, S. Cai, A porous Cu/LDPE composite for copper-containing intrauterine contraceptive devices, Acta Biomater. 8 (2) (2012) 897–903.
- [67] J.M. Bastidas, E. Cano, N. Mora, Copper corrosion-simulated uterine solutions, Contraception 61 (6) (2000) 395–399.
- [68] X.X. Xu, F.L. Nie, Y.B. Wang, J.X. Zhang, W. Zheng, L. Li, Y.F. Zheng, Effective inhibition of the early copper ion burst release with ultra-fine grained copper and single crystal copper for intrauterine device application, Acta Biomater. 8 (2) (2012) 886–896.
- [69] N. Mora, E. Cano, E.M. Mora, J.M. Bastidas, Influence of pH and oxygen on copper corrosion in simulated uterine fluid, Biomaterials 23 (3) (2002) 667–671.
- [70] H. K., Intrauterine contraception with the copper-T device. 4. Influence on protein and copper concentrations and enzyme activities in uterine washings, 6(3) (1972) 219–30.
- [71] E. Johannisson, Mechanism of action of intrauterine devices: biochemical changes, Contraception 36 (1) (1987) 11–22.
- [72] J.A. Spinnato 2nd, Mechanism of action of intrauterine contraceptive devices and its relation to informed consent, Am. J. Obstet. Gynecol. 176 (3) (1997) 503–506.
- [73] K. Takeuchi, A. Mori, S. Yamamoto, T. Sonoda, Y. Nagata, Effect of the secretions from the IUD-bearing uterus on peri-implantation mouse embryos, Contraception 41 (6) (1990) 655–662.
- [74] V. Arancibia, C. Pena, H.E. Allen, G. Lagos, Characterization of copper in uterine fluids of patients who use the copper T-380A intrauterine device, Clin. Chim. Acta 332 (1–2) (2003) 69–78.
- [75] B.I. Baranowska, I. Gutowska, C. Marchetti, Altered energy status of primary cerebellar granule neuronal cultures from rats exposed to lead in the pre- and neonatal period, Toxicology 280 (1–2) (2011) 24–32.
- [76] M.F. Braga, E.F. Pereira, A. Mike, Pb2+ via protein kinase C inhibits nicotinic cholinergic modulation of synaptic transmission in the hippocampus, J. Pharmacol. Exp. Ther. 311 (2) (2004) 700–710.
- [77] J.L. Tomsig, J.B. Suszkiw, Multisite interactions between Pb2+ and protein kinase C and its role in norepinephrine release from bovine adrenal chromaffin cells, J. Neurochem. 64 (6) (1995) 2667–2673.
- [78] D. Beyersmann, Interactions in metal carcinogenicity, Toxicol. Lett. 72 (1–3) (1994) 333–338.